ACS APPLIED ENERGY MATERIALS

November 11, 2024
Volume 7
Number 21
pubs.acs.org/acsaem

ACS Publications
Most Trusted. Most Cited. Most Read.

www.acs.org

ACS APPLIED ENERGY MATERIALS

www.acsaem.org Article

Tailoring the Transport Layer Interface for Relative Indoor and Outdoor Photovoltaic Performance

Chia-Feng Li, Shih-Han Cheng, Hou-Chin Cha, Ssu-Yung Chung, Damian Glowienka, Chih-Min Chuang, and Yu-Ching Huang*

Cite This: *ACS Appl. Energy Mater.* 2024, 7, 10203−10211 Read Online

ACCESS | Metrics & More | Article Recommendations | Supporting Information

ABSTRACT: The ability to achieve notable indoor power conversion efficiency (PCE) makes organic photovoltaics (OPV) a potential technology for indoor applications. Currently, ongoing research in indoor OPVs focuses on improving both their indoor PCE and their stability. However, little attention has been given to investigating the fabrication yield of indoor OPVs, a pivotal determinant of their potential commercial viability. In this study, we discovered that despite assessing the PCE of OPVs under indoor and solar illumination conditions using the same devices, the fabrication yields under these distinct light sources vary significantly. Employing diverse analytical measurements, we elucidated the underlying mechanisms contributing to this variance. Our findings suggest that disparities in fabrication yield resulted from the interfacial interactions between the hole transport layer (HTL) and the active layer. Particularly, the interfacial behavior between these layers plays a decisive role in achieving elevated fabrication yields in indoor OPVs. Furthermore, we demonstrate the function of a combination of two HTLs (TAPC/MoO_3), which not only enhances the indoor PCE of OPVs but also substantially improves the fabrication yield of indoor OPVs. Our study offers insights and critical guidance for the advancement of indoor OPVs with high fabrication yields.

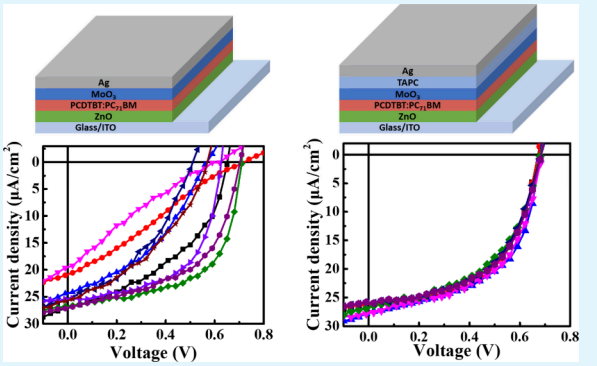

KEYWORDS: *organic photovoltaics, indoor light, fabrication yield, hole transport layer, interfacial behavior*

INTRODUCTION

Recently, the pursuit of efficient and environmentally friendly energy solutions has led to significant advancements in the field of organic photovoltaics (OPVs). Organic materials present unique properties and versatility garnering substantial interest due to the advantages of low cost, mechanical flexibility, lightweight, and solution processability. As an emerging renewable energy, OPV has achieved a power conversion efficiency (PCE) of up to ∼20% under sunlight due to the utilization of novel low bandgap polymer donor and non-fullerene acceptor (NFA) materials in the active layer.[1−7] However, the PCE of OPV is profoundly influenced by the application conditions, such as heat, moisture, illumination, and their combination. Thus, facile and powerful strategies for simultaneously enhancing the efficiency and stability of OPVs are still being developed. With regard to the issues mentioned above, recent studies have explored the role of interfacial morphology,[8−10] intermolecular interactions,[11−14] and energy level alignments in governing charge transport,[15,16] and overall device stability,[17] providing an in-depth analysis of the relationship between intrinsic mechanisms and performance. Additionally, organic materials are easy to control the absorption region via molecular design and have high absorption coefficients in the visible light range that closely match the broad light spectrum,[18−23] making them feasible for indoor applications. The PCE of OPV devices is mainly determined by the surrounding illumination conditions, which can vary widely from natural sunlight to artificial lighting sources. Because of the rapid development of OPVs under solar illumination in recent years, OPVs under indoor lighting have also received significant attention and have made relative progress. Hence, recent research endeavors have strived to engineer OPVs with a relative performance under solar and artificial illumination. The theoretical indoor efficiency of an OPV can reach up to 60%, whereas OPVs have already achieved an indoor PCE of around 30% and thus still do not reach the maximum values.[24−29]

Many research teams have employed various strategies to improve the PCE of OPVs under sunlight, including selecting materials to increase light absorption, tuning the fabrication process to optimize interfacial contact, and utilizing annealing

Received: October 7, 2024
Revised: October 22, 2024
Accepted: October 28, 2024
Published: October 31, 2024

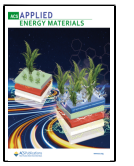

and additives to improve the internal nanostructure and morphology. The performance differences of OPVs under sunlight and indoor light conditions have been broadly discussed. Generally, under solar illumination the short current density (J_{SC}) and fill factor (FF) of OPVs are significantly affected by the series resistance (Rs), while the shunt resistance (R_{sh}) is less significant due to inverse relation to photocurrent. On the contrary, under indoor light conditions with reduced light intensity, the decrease of J_{SC} reduces the effect of Rs on the indoor PCE, and instead, OPVs with high R_{sh} can show good indoor PCE.[30] Moreover, our recent study has also highlighted the critical role of R_{sh}, monomolecular recombination, and trap depth in influencing the indoor PCE of OPVs.[31] For indoor OPVs, increasing the open circuit voltage (V_{OC}) value of the OPV is particularly crucial for achieving high indoor PCEs. Yang et al. have demonstrated that by augmenting the energy gap between the highest occupied molecular orbital (HOMO) of the donor material and the lowest unoccupied molecular orbital (LUMO) of the acceptor material, P3HT:ICBA exhibits an elevated V_{OC}, consequently yielding a PCE of 13.76% under 500 lx indoor light illumination.[32] Furthermore, NFAs with higher LUMO than fullerene derivative acceptors can reduce V_{OC} losses and exhibit better absorption in visible light, leading to higher J_{SC}. Cui et al. have elucidated a photoactive layer consisting of IO-4Cl with PBDB-TF with a suitable absorption spectrum for indoor lighting sources.[33] The bulk heterojunction (BHJ) structured device with an area of 1 cm^2 demonstrated a PCE of 9.8%, along with V_{OC} of 1.24 V, J_{SC} of 11.6 mA/cm^2, and fill factor (FF) of 68.1% under 1 sun illumination.[25] When exposed to LED illumination at 2700 K, the devices exhibited PCEs of 22.2%, 24.6%, and 26.1% at 200, 500, and 1000 lx, respectively. In addition to the active layer, the effect of the charge transport layer on the performance of indoor OPVs has been evaluated. Ma et al. investigated the differences in PCE under different light sources for OPVs with varying electron transport layers (ETLs). Here, the OPV used two ETL materials, PDINO and PFN, where PDINO has a deeper HOMO than PFN. Both OPVs performed similarly under sunlight; however, the OPVs fabricated from PDINO exhibited a higher indoor PCE (~31%) than those using PFN (~27%) under indoor lighting conditions. This is mainly because ETLs with a deeper HOMO effectively prevent hole injection into the active layer and reduce the leakage current. In some studies, including the work by Xie et al., SnO_X was grown on silver nanowires (AgNWs) to form core−shell electrodes, enhancing the performance of flexible indoor OPVs. The AgNWs were treated with $SnCl_2$, which not only generated SnO_X but also removed surface defects. This SnO_X layer improved the stability and adjusted the work function of the AgNWs, enabling efficient charge injection and collection. Consequently, the AgNWs@ SnO_X electrode achieved an impressive efficiency of 25.51% under 1000 lx illumination compared to the 18.84% efficiency of the AgNWs electrode alone.[34] In our previous study,[35] we investigated the impact of ZnO prepared through various processes as the ETL in OPVs on the PCE under two different light sources. Our results show that although all ETLs are ZnO, their differences in surface morphology, internal defects, and crystallinity still lead to different PCE under solar and indoor light illuminations. In addition, we reveal that surface defects in the ETLs are critical factors influencing the indoor PCE of OPVs.

The impressive progress in the PCE of OPVs has raised important research topics regarding the feasibility of commercial production. These include the development of large-area deposition process,[36−38] modularization technologies,[39−41] and thorough evaluations of device stability.[42−44] However, there is a significant lack of research on the fabrication yields of devices, which is a crucial technology for advancing toward the commercial mass production of OPVs. Mitra et al. demonstrated that in fully inkjet-printed OPVs, variations in the morphology of the lower active layer, P3HT:PCBM, result in significant surface topology deviations in the upper PEDOT:PSS layer. This discrepancy leads to a substantial variation in PCE, i.e., low fabrication yield, of OPVs even fabricated within the same batch. By optimizing the morphology of the lower active layer, they were able to increase the fabrication yield of large quantities and various sizes of flexible OPVs to more than 70%.[45] Che et al. demonstrated that the fabrication yield of tandem cells can be effectively improved by more than 95% by controlling the hydrophilic−hydrophobic interface within the charge recombination zone connecting the two subcells.[46] Additionally, in our previous study, by controlling the ratio of two solvent additives, we enabled the fabrication of slot-die-coated OPVs within a broader substrate temperature processing window, which substantially improved the fabrication yields of the OPVs in different batches.[47] However, the aforementioned studies mainly focus on OPVs under sunlight illumination, and there are no studies in the literature related to the fabrication yield of indoor OPVs. In this study, we focus on the key factors affecting the fabrication yields of indoor OPVs. We use the commonly used thermal evaporated MoO_3 as HTL to investigate how the HTL affects the fabrication yield of the indoor OPVs. By controlling the processing conditions of MoO_3, including the deposition rate and vacuum level during the thermal evaporation, we found that the interaction between the active layer and the HTL plays a pivotal role in the fabrication yield of indoor OPVs. Furthermore, we introduce a combination of two HTLs, 1,1-bis[(di-4-tolylamino)phenyl]-cyclohexane (TAPC) and MoO_3, to reduce the energy loss at the interface between the active layer and the metal electrode of the OPVs and passivate the oxygen vacancies in MoO_3 by TAPC to facilitate hole extraction from the active layer of the OPVs, which dramatically improves the fabrication yields of the indoor OPVs.

METHODOLOGY

Materials. Zinc acetate dihydrate (≥98%), ethanolamine (MEA, 98%), 2-methoxyethanol (2-ME, 99.8%), *o*-xylene (≥99.8%), 2-propanol (99.5%), and acetone (99.5%) were purchased from Sigma-Aldrich. Poly[*N*-11″-henicosanyl-2,7-carbazole-*alt*-5,5-(4′,7′-di-2-thienyl-2′,1′,3′-benzothiadiazole)] (PCDTBT) was obtained from 1-Materials. Poly[(2,6-(4,8-bis(5-(2-ethylhexyl-3-fluoro)thiophen-2-yl)-benzo[1,2-b:4,5-*b*0]dithiophene))-*alt*-(5,5-(10,30-di-2-thienyl-50,70-bis(2-ethylhexyl)benzo[10,20-*c*:40,50-*c*0]dithiophene-4,8-dione)] (PM6) and non-fullerene acceptor material, 2,2′-[[12,13-bis(2-ethylhexyl)-12,13-dihydro-3,9-diundecylbisthieno[2″,3″:4′,5′]-thieno[2′,3′:4,5]pyrrolo[3,2-*e*:2′,3′-*g*][2,1,3]benzothiadiazole-2,10-diyl]bis[methylidyne(5,6-difluoro-3-oxo-1H-indene-2,1(3*H*)-diylidene)]]bis[propanedinitrile] (Y6), were supplied by 1-Materials. Indium-doped tin oxide (ITO), (6,6)-phenyl C_{71} butyric acid methyl ester ($PC_{71}BM$), and 1,1-bis[(di-4-tolylamino)phenyl]cyclohexane (TAPC) were obtained from

https://doi.org/10.1021/acsaem.4c02521
ACS Appl. Energy Mater. 2024, 7, 10203−10211

Luminescence Technology. Molybdenum(VI) oxide (MoO_3, 99.9995%) was purchased from Alfa Aesar. Ag was purchased from Gredmann Taiwan Ltd. All chemicals were used as received without any further treatment.

Device Fabrication. The ITO substrates were sequentially cleaned with detergent, deionized water, acetone, and 2-propanol using an ultrasonic cleaner for 20 min each, followed by UV ozone treatment of the ITO substrates for 30 min. The sol−gel ZnO precursor solution was prepared by dissolving 1 g of zinc acetate dihydrate and 0.28 g of ethanolamine in 10 mL of 2-methoxyethanol, and the mixture was stirred overnight to ensure complete dissolution and a homogeneous solution. The sol−gel ZnO precursor solution was spin-coated at 3000 rpm for 30 s and then annealed at 180 °C for 20 min. PCDTBT:$PC_{71}BM$ was dissolved in *o*-xylene in a ratio of 1:2 by weight at a total concentration of 21 mg/mL and stirred at 70 °C overnight to obtain the active layer. PM6:Y6 was dissolved in chloroform in a ratio of 1:1.2 by weight at a total concentration of 17.6 mg/mL and stirred at 40 °C for 1 h. The active layers of PCDTBT:$PC_{71}BM$ and PM6:Y6 were deposited onto the ZnO film by spin coating at 1000 and 5000 rpm for 30 s in a glovebox, respectively. Finally, the HTL and silver electrode were thermal evaporated sequentially on the active layer.

Device Characterization. The characteristics of the OPVs were measured by a voltage source meter (Keithley 2410) under a 3A class AM 1.5G solar simulator (Enli Tech, SS-X100R) with an irradiation of 100 mW/cm^2 (represents outdoor illumination). The performance of the OPV under indoor light was measured by an integrated system (Industrial Technology Research Institute, ITRI) composed of a power meter (Keithley 2401) and a light source of Philips TLD 18W/830. The intensity of indoor light can be modulated to 300 and 1000 lx, which corresponds to 0.087 and 0.290 mW/cm^2. The morphology of the surface of the films was obtained using atomic force microscopy (AFM; Bruker). The impedance measurements were conducted by electrochemical impedance measurement (Material Lab XM module). The work function of the film was determined using a scanning Kelvin probe (KP Technology SKP5050), a specialized surface analysis tool designed to directly assess variations in work function and surface potential on solid surfaces.

RESULTS AND DISCUSSION

To investigate the relative performance of OPVs under outdoor and indoor lighting, we fabricated OPV devices with the structure ITO/ZnO/PCDTBT:$PC_{71}BM$/MoO_3/Ag. The MoO_3 HTL was deposited at different evaporation rates of 0.5 and 0.1 Å/s, with a thickness of 8 nm, while the thickness of the Ag layer was 100 nm. Figure 1 shows the current density−voltage (*J*−*V*) curves of the OPVs observed under 1 sun and indoor illumination. Four identical samples were fabricated, and eight devices on each sample were measured for PCE to obtain precise data. As shown in Figure 1a,b, under 1 sun illumination, the devices demonstrated efficient performance with good repeatability regardless of the deposited rate of MoO_3. In comparison to OPVs illuminated under 1 sun, the performance of OPVs illuminated under indoor light is quite different. As shown in Figure 1c,d, the indoor PCE of devices is still relatively stable for the devices with a MoO_3 evaporation rate of 0.1 Å/s, but the indoor PCE shows significant fluctuations for the devices with a MoO_3 evaporation rate of 0.5 Å/s. We further conducted experiments by the devices with

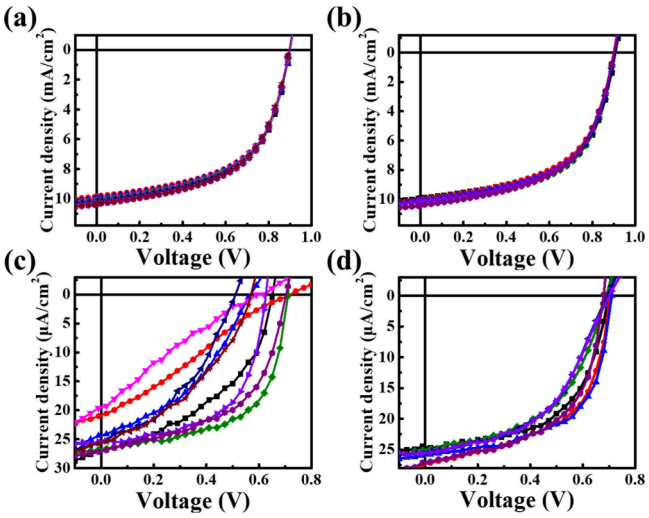

Figure 1. *J*−*V* curves of OPVs with different evaporation rates of MoO_3 material: (a) 0.5 and (b) 0.1 Å/s under l sun illumination and (c) 0.5 and (d) 0.1 Å/s under indoor illumination.

MoO_3 films deposited under different vacuum degree, and the relevant results are shown in Figure S1. Our results demonstrate that when MoO_3 is deposited in a suboptimal vacuum environment (8×10^{-6} Torr), OPVs exhibit unstable indoor PCE, although the same devices exhibit similar PCE under 1 sun illumination. However, even when MoO_3 is deposited under different vacuum conditions, the OPVs show comparable and uniform PCE under 1 sun illumination. This suggests that various MoO_3 fabrication parameters do significantly affect the indoor performance of the OPVs and to a lesser extent the 1 sun performance, ultimately reducing the fabrication yields of indoor OPVs. We propose that the inhomogeneous arrangement of MoO_3 materials caused by a rapid evaporation rate or insufficient vacuum during the thermal evaporation process leads to significant instability of OPVs under indoor illumination. Furthermore, there are pinholes for the active layer due to the inhomogeneous MoO_3 layer, thus creating the shunts. It results in lowering the shunt resistance at insufficient vacuum pressure. This is not visible under 1 sun conditions but is observable under indoor conditions.

We first analyzed the surface morphology of the films deposited at different evaporation rates using AFM. The PCDTBT:$PC_{71}BM$ film exhibits a root-mean-square (RMS) roughness of 2.72 nm (Figure 2a). After the deposition of MoO_3 HTL prepared at a deposition rate of 0.5 Å/s, the roughness of the film increased to 3.12 nm (Figure 2b). This could be a factor causing significant fluctuations in the PCE of indoor OPVs. When a deposition rate of 0.1 Å/s was used, the roughness of the film decreased to 3.01 nm (Figure 2c). A slower deposition rate helps in forming a uniform film layer, providing more consistent optical and mechanical properties. Additionally, a slower deposition rate results in lower internal stress, which can improve the adhesion and stability of the film and enhance the quality of the interface contact between the film and the metal electrode. Thus, the fluctuations in the PCE of indoor OPVs can be mitigated. This phenomenon can be further explained by the significantly higher surface energy of MoO_3 compared with organic materials. Generally, a larger water contact angle indicates a smaller surface energy of the material, and vice versa.[48,49] To understand the surface energy

https://doi.org/10.1021/acsaem.4c02521
ACS Appl. Energy Mater. 2024, 7, 10203−10211

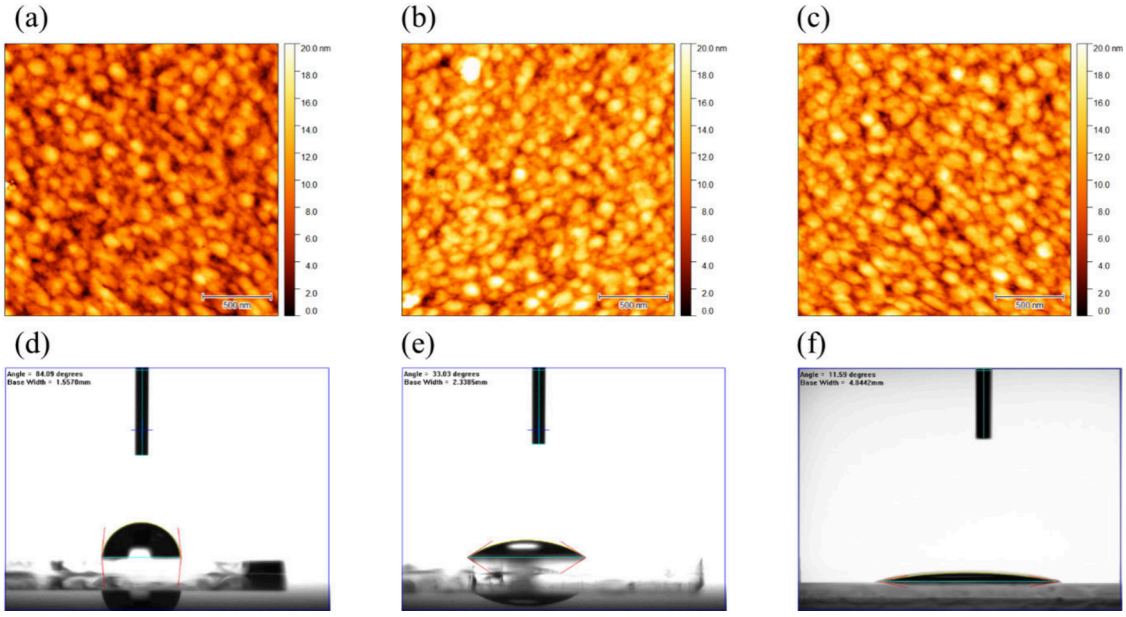

Figure 2. AFM topographical images of the PCDTBT:$PC_{71}BM$ film (a) without HTL, (b) with MoO_3 HTL (0.5 Å/s), and (c) with MoO_3 HTL (0.1 Å/s). Water contact angle images of (d) PCDTBT:$PC_{71}BM$ film, (e) MoO_3 film (0.5 Å/s), and (f) MoO_3 film (0.1 Å/s) on a glass substrate.

difference between the materials, we conducted related measurements using water contact angles. Figure 2d,e illustrates the water contact angles of the active layer PCDTBT:$PC_{71}BM$ and the MoO_3 film prepared at a deposition rate of 0.5 Å/s measuring 84.09° and 33.03°, respectively. Additionally, the corresponding surface energies were found to be 7.519 and 61.20 mN/m. A large difference in surface energy between the two materials will lead to MoO_3 atoms tending to adsorb each other, leading to the formation of discontinuous and rough films, known as the famous Volmer−Weber film growth mechanism.[50] However, when the MoO_3 film is prepared at a deposition rate of 0.1 Å/s, the measured water contact angle further decreases to 11.59° (Figure 2f), and the corresponding surface energy increases to 83.74 mN/m. The slower deposition rate results in a greater difference in surface energy relative to that of the active layer, which could potentially cause adverse effects. However, this does not appear to cause fluctuations in the PCE of indoor OPVs. We speculate that the slower deposition rate helps in forming an ordered lattice structure and reduces the internal defect density of the MoO_3 film, allowing efficient hole extraction and transport. Moreover, the shunt effect of OPV devices under indoor illumination appears to be inhibited by a slower evaporation rate or higher vacuum levels, reducing the leakage current and thereby minimizing fluctuations in the PCE of indoor OPVs. This hypothesis will be verified in subsequent experiments.

To further investigate the difference in PCE of the various HTLs for OPVs under 1 sun and indoor light illuminations, we measured the interfacial behavior between the active layer and the MoO_3 layer using impedance spectroscopy. Figures 3a and 3b show the corresponding Nyquist plots obtained from impedance measurements of the OPVs under short-circuit conditions,[51,52] which can be simulated with a simple parallel resistor−capacitor (RC) circuit (Figure 3c). Using the equivalent circuit model shown in Figure 3c, the fitted parameters are listed in Table S1. *Rs* represents the series resistance of the device, while the combination of R1 and C1

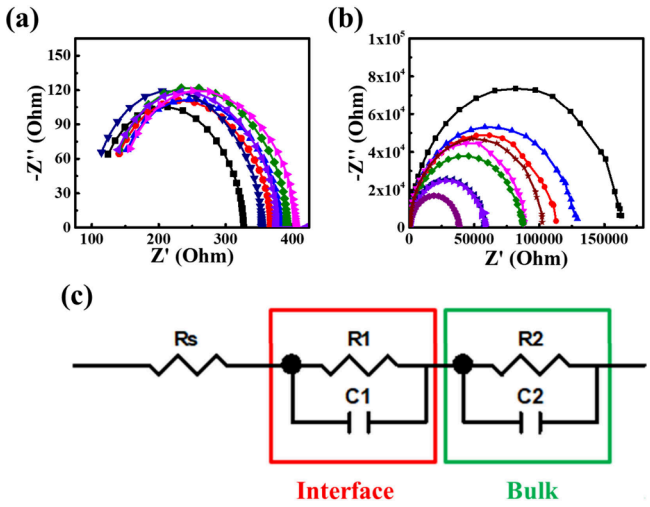

Figure 3. Complex impedance plots (Nyquist plot) of PCDTBT:$PC_{71}BM$ OPV measured under (a) 1 sun illumination, (b) indoor illumination, and (c) simple parallel resistor−capacitor circuit of the BHJ OPV.

corresponds to the interfacial resistance and capacitance between the active layer and the charge transport layer. Meanwhile, the pairing of R2 and C2 reflects the charge transfer resistance and diffusion capacitance within the bulk heterojunction (BHJ) active layer. According to previous literature,[51] the two processes observed in the impedance response are associated with the recombination in the active layer at high frequency and the interlayer resistance and capacitance at low frequency. As shown in Figure 3, the difference in the low-frequency behavior of the same devices under different illumination is the most obvious, representing that the interlayer impedance behavior of the MoO_3 layer is indeed greatly varied by different illumination. Figure 3a shows the results of the devices measured under 1 sun, which reveal relatively small and uniform semicircles at a low frequency. Whereas, when the same devices are measured under indoor

https://doi.org/10.1021/acsaem.4c02521
ACS Appl. Energy Mater. 2024, 7, 10203−10211

light (Figure 3b), it is obvious that the Nyquist plots show a much larger semicircle, and the interfacial impedance behavior of devices under indoor light is extremely different. This result suggests that when the contact between the MoO_3 layer and the active layer is poor, the devices illuminated under indoor light show an increase in the charge transfer resistance, leading to obvious interfacial charge recombination, which in turn affects the PCE and fabrication yield of indoor OPVs. However, this phenomenon is almost negligible when the same devices are illuminated by 1 sun.

Here, we propose a combination of two HTLs (TAPC/MoO_3, named bilayer HTL), where the TAPC film, with a thickness of 5 nm, acts as an interfacial layer between the MoO_3 layer and the active layer to solve the interfacial contact issue. First, by introducing the TAPC layer between the active layer and MoO_3 layers, a reduced roughness of 2.35 nm was obtained from the AFM image, which indicated a smooth morphology of the MoO_3 film and a good interfacial contact between the MoO_3 and the metal electrode (Figure S2a). Additionally, the TAPC layer exhibits a water contact angle of 54.26° (Figure S2b) and a corresponding surface energy of 42.64 mN/m, exhibiting a higher surface energy compared to PCDTBT:$PC_{71}BM$ and being closer to that of MoO_3. This result implies that utilizing TAPC as an intermediate layer can alleviate the surface energy disparity between the polymer and inorganic materials. However, after the addition of the TAPC layer, MoO_3 has the potential to follow the Frank−van der Merwe growth mechanism, enabling the formation of a continuous, flat, and defect-free thin film.[53] Furthermore, the schematic diagram in Figure S2c depicts the change in the work function after the addition of the TAPC layer as well as the energy level diagram for the two HTLs. According to the calculations, the work function of MoO_3 is about 5.10 eV, whereas after the TAPC modification, the work function changes subtly to about 5.15 eV. We suggest that the introduction of TAPC results in a proper alignment of the energy levels at the interface, which is essential for minimizing the energy barriers and facilitating charge transfer, thus preventing charge accumulation and reducing recombination at the interface.

We further compare the effect of the bilayer HTL on the fabrication yield of indoor OPVs. It is worth noting that the TAPC layer was deposited at an evaporation rate of 0.1 Å/s and an identical vacuum degree as the MoO_3 layer deposition (8×10^{-6} Torr). As shown in Figure 4, the introduction of the bilayer HTL layer dramatically reduces the instability of indoor photovoltaic characteristics, including PCE, V_{oc}, J_{sc}, and FF, of the OPVs. The $J-V$ curves of the indoor OPVs fabricated from the bilayer HTL (Figure 4e) displays excellent overlap as compared to the OPVs fabricated from single HTL in Figure 1c. Moreover, Figure S3 reveals that the OPVs with bilayer HTL exhibit a PCE compatible with the OPVs with single HTL under 1 sun illumination. This result suggests that the introduction of the TAPC/MoO_3 bilayer HTL improves the fabrication yield of the OPVs under indoor light without affecting the PCEs of the devices under 1 sun and indoor light. The values of the PCE, V_{OC}, FF, and J_{SC} of the OPVs measured under 1 sun and indoor light are listed in Tables S2 and S3, respectively. This improvement under indoor light illumination may be related to the reduction of contact resistance and is also reflected in the enhanced charge extraction and transport capability. Additionally, the lower voltage loss contributes to the suppression of recombination behavior at the interface.

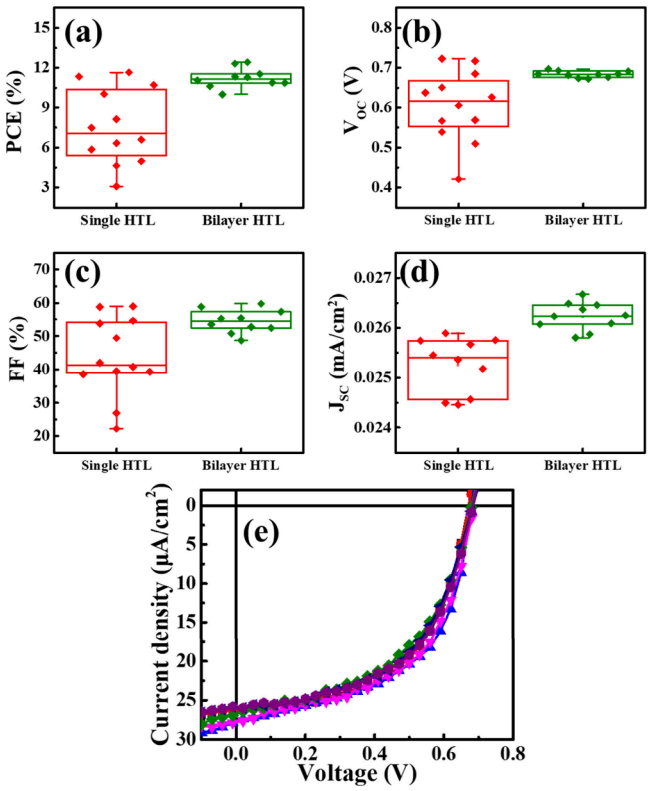

Figure 4. (a) PCE, (b) V_{OC}, (c) FF, and (d) J_{SC} of the PCDTBT:$PC_{71}BM$ OPV device with the single and bilayer HTLs measured under indoor illumination. (e) $J-V$ curve of the PCDTBT:$PC_{71}BM$ OPV device with the bilayer HTL measured under indoor illumination.

From the results presented above, the introduction of a bilayer HTL improves the interfacial behavior between the active layer and the metal electrode and promotes effective hole transport under indoor illumination. The improvement of devices with the bilayer HTL under indoor illumination can be further explained by the impedance spectroscopy, which is shown in Figure S4. Figures S4a and S4b show the Nyquist plots of the devices based on bilayer HTL under 1 sun illumination and indoor illumination, respectively. The impedance behavior of the devices under 1 sun is similar to that of the devices based on a single HTL. In contrast, under indoor light illumination, the Nyquist plots of the OPVs with the bilayer HTL exhibit a noticeably smaller and more uniform semicircle along the real axis than those of the devices with a single HTL. This implies a significant reduction in the interfacial impedance of the devices, effectively reducing the recombination behavior at the interface and thus significantly improving the low fabrication yield of indoor OPVs.

We further explore the effects of the TAPC layer on the carrier lifetime and the carrier extraction time of the OPVs by using transient photovoltage (TPV) and transient photocurrent (TPC) measurements, respectively.[54] Figure 5a shows the TPV of the OPVs measured at open circuit condition under indoor illumination, and we can observe that the charge decay time of the OPVs changes from 49.93 to 40.30 μs when the HTL changes from single HTL to bilayer HTL. While this change indicates a difference in charge decay time, it does not result in a significant impact on the performance of the indoor OPVs based on bilayer HTL. Figure 5b displays the TPC of the OPVs measured at short-circuit condition under indoor

https://doi.org/10.1021/acsaem.4c02521
ACS Appl. Energy Mater. 2024, 7, 10203−10211

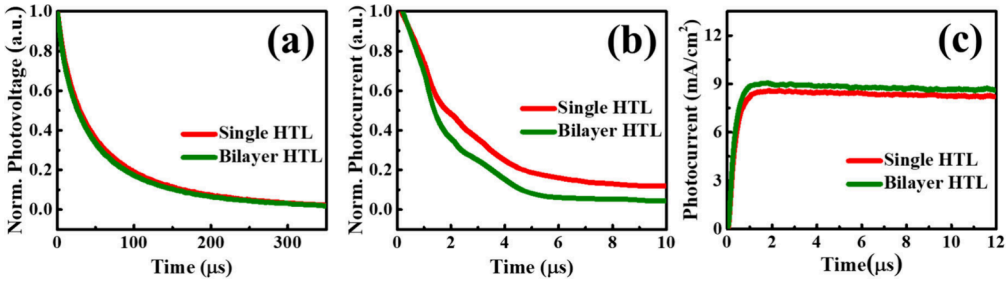

Figure 5. (a) Normalized transient voltage, (b) normalized transient current, and (c) Photo-CELIV curves of the OPV device with the single and the bilayer HTLs measured under an indoor lamp.

illumination, demonstrating an evident decrease in the charge extraction time (from 2.58 to 2.12 μs) following the introduction of the bilayer HTL. This decrease in the charge extraction time in the devices indicates that the OPVs with bilayer HTL possess a faster charge transfer as compared to the devices with the single HTL. The charge mobility is further observed through photogenerated charge carriers by linear increasing voltage (Photo-CELIV) measurements (Figure 5c). The Photo-CELIV curves of OPV reveal that OPV demonstrates a carrier mobility of ~3.72 × 10^{-5} $cm^2/(V\ s)$ while upon addition of TAPC the carrier mobility of the device increased to ~4.27 × 10^{-5} $cm^2/(V\ s)$. The improved mobility in OPVs is suggested to be attributed to the proper formation of the MoO_3 layer due to the mediation of the TAPC. Figure S5 illustrates the carrier behavior and mobility of the OPVs under 1 sun illumination, and these results are consistent with the result in Figure 5, validating that the introduction of the TAPC enables more efficient charge transport behavior. Table S4 lists the calculated values of carrier behavior and mobility of OPVs under the two light sources illuminations.

To correlate the effectivity of the bilayer HTL on the OPVs for the relative performance in outdoor and indoor environments, a detailed analysis of the bimolecular and monomolecular recombination behaviors was measured.[31,35,55] The V_{OC} and J_{SC} of the OPVs were measured under various light intensities, as shown in Figure 6. Figure 6a displays the V_{OC}

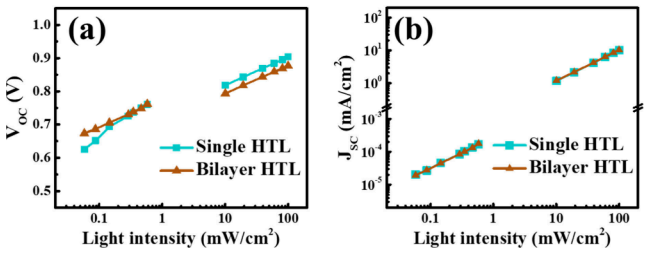

Figure 6. (a) Mono- and (b) bimolecular recombination of the OPVs with the single-layer and bilayer HTLs measured under 1 sun and TL84 indoor light illuminations.

values measured at an open circuit under various light intensities, where all carriers are assumed to recombine completely. This behavior is described by the equation $V_{OC} \propto nkT/q \ln I$, where n represents the slope of the V_{OC} versus light intensity curve, k represents the Boltzmann constant, T represents temperature, and q represents the elementary charge. In addition, n = 1 indicates a decrease in trap-assisted recombination in the device, and Table S5 lists the n values measured from V_{OC} of the OPVs. Under the 1 sun condition, a negligibly small change in n can be observed for the OPVs with the single- and bilayer HTLs, indicating that a comparable amount of trap states is present in the two devices. However, under indoor illumination, the OPVs with the single HTL exhibit a higher n value than that of devices with the bilayer HTL, indicating the presence of a higher trap state in indoor condition. In addition, the n of the devices with bilayer HTL is very close to 1 under indoor light, representing that the devices exhibit the lowest trap-assisted recombination. According to our previous literature, trap-assisted recombination is the dominant factor for the indoor PCE of OPVs.[28,31] Figure 6b illustrates the J_{SC} measured under different light intensities, and the relationship between the J_{SC} and light intensity can obtain further insight into the different states of recombination by using the power law of $J_{SC} \propto I^{\alpha}$, where I is the light intensity, and an α close to unity implies a weak bimolecular recombination. The α values of the OPVs fabricated from the single-layer and bilayer HTLs are listed in Table S5. Under 1 sun illumination, the OPVs show similar α values regardless of the introduction of the TAPC layer. Likewise, a similar α value was obtained under indoor illumination, suggesting comparable carrier transport and carrier collection efficiencies in the devices.

Finally, we used indoor fluorescent lamp (TL84) with a light intensity of 1000 lx (~0.29 mW/cm^2) for 24 h to evaluate the changes in the OPVs under prolonged illumination in an indoor light environment, and the results are shown in Figure 7. Figures 7a and 7d show the $J-V$ curves of the as-fabricated devices, and it can be found that there is still a serious fabrication yield problem with the devices fabricated from the single HTL, which can be greatly improved by using a bilayer HTL instead of a single HTL. Then we put these devices under the TL84 light illumination for 24 h, and the $J-V$ curves of the devices with single HTL and with bilayer HTL are shown in Figures 7b and 7e, respectively. It is worth noting that after 24 h of continuous exposure to TL84 light, the original low fabrication yield of devices shows a significant improvement. We infer that this improvement is due to the fact that the OPVs fabricated from the single HTL exhibit more defects, which serve as traps, leading to increased trap-assisted charge recombination. However, after long-term continuous exposure to indoor light, the light-induced carriers gradually fill these traps, facilitating effective charge extraction and transport. This process mitigates the indoor PCE differences between the devices, resulting in a significant improvement in the fabrication yields of the OPVs with single HTL. However, after moving these illuminated devices to dark storage for 24 h, the devices with the single HTL exhibited divergent $J-V$ curves once again, as shown in Figure 7c. We inferred that this is because the traps at the interface of the devices revert to their original state after dark storage, resulting in a low

https://doi.org/10.1021/acsaem.4c02521
ACS Appl. Energy Mater. 2024, 7, 10203−10211

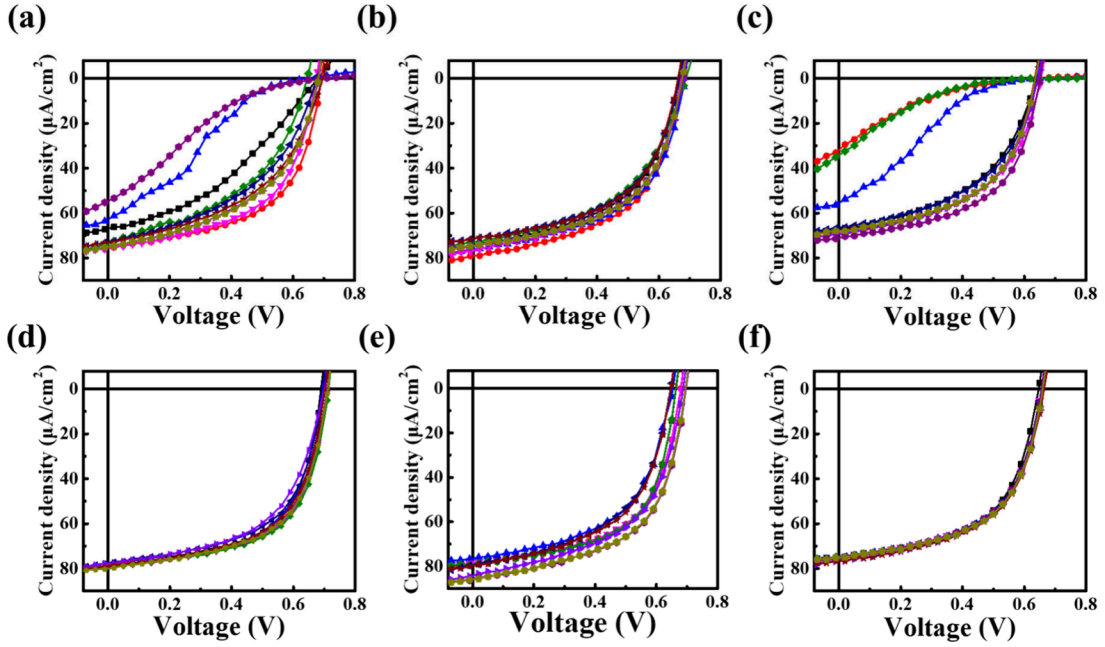

Figure 7. $J-V$ curves of as-prepared OPV devices with the (a) single HTL and (d) bilayer HTL, followed by the devices with the (b) single HTL and (e) bilayer HTL after 24 h of continuous illumination under a fluorescent lamp and the devices with the (c) single HTL and (f) bilayer HTL followed by 24 h of dark storage.

fabrication yield of the indoor PCEs. In contrast, the OPVs fabricated with bilayer HTL maintain good consistency in indoor PCEs in initial fabrication, long-time illumination, and subsequent dark storage (Figure 7f), which confirms that the bilayer HTL is highly effective in improving the fabrication yield and stability of indoor OPVs.

Furthermore, to assess the generality of using a bilayer HTL in enhancing the performance as well as the fabrication yield of indoor OPVs, we employed additional donor−acceptor blends, PM6:Y6, as the active material system. The values of the PCE, V_{OC}, FF, and J_{SC} of the OPVs with a MoO_3 evaporation rate of 0.5 Å/s measured under indoor illumination are listed in Table S6. The $J-V$ curves of the indoor OPVs fabricated with the bilayer HTL (Figure S6) display excellent overlap compared to the OPVs fabricated with a single HTL. It is apparent that indoor OPVs, due to differences in fabrication conditions, often suffer from poor fabrication yield under indoor illumination. Therefore, the strategies proposed in this study can increase the tolerance of fabrication parameters, thereby perfectly addressing this issue.

CONCLUSION

This study delves into the critical impact of the interfacial interactions between the hole transport layer and the active layer on organic photovoltaics under different illumination conditions. The results show that although the efficiency and fabrication yield of OPV devices do not vary with different HTL combinations and fabrication conditions under sunlight, achieving good performance for indoor OPVs requires well-designed interfacial layers. We demonstrated the effectiveness of a bilayer HTL, which promotes efficient charge extraction and transfer between the layers in the device. This phenomenon is also validated by the lower resistance observed in electrochemical impedance spectroscopy measurements. Furthermore, the bilayer HTL forms fewer defects, significantly reducing the probability of trap-assisted recombination. Notably, this proposed HTL design significantly improves the inconsistent performance of indoor OPVs using a single HTL under indoor lighting conditions. These advancements are attributed to the bilayer HTL aiding in uniform film formation and defect passivation. Moreover, these OPV devices exhibit superior stability under indoor lighting conditions, maintaining consistent $J-V$ curves even under light and dark storage cycling operations. Finally, this study is the first to analyze the fabrication yield of OPV devices under indoor lighting conditions. It not only provides valuable insights into HTL materials for indoor photovoltaic applications but also enhances the feasibility of this technology for commercial mass production, paving the way for future advancements in the indoor OPV field.

ASSOCIATED CONTENT

Supporting Information

The Supporting Information is available free of charge at https://pubs.acs.org/doi/10.1021/acsaem.4c02521.

Performance plot, water contact angle images, energy level schematic diagram, resistance−capacitance schematic diagram, Nyquist plot, normalized transient photocurrent, normalized transient photovoltage, Photo-CELIV curves, and table for all calculated values (PDF)

AUTHOR INFORMATION

Corresponding Author

Yu-Ching Huang − *Department of Materials Engineering, Ming Chi University of Technology, New Taipei City 24301, Taiwan; Department of Chemical and Materials Engineering, Chang Gung University, Taoyuan 33302, Taiwan;* orcid.org/0000-0003-4772-8050; Email: huangyc@mail.mcut.edu.tw

https://doi.org/10.1021/acsaem.4c02521
ACS Appl. Energy Mater. 2024, 7, 10203−10211

Authors

Chia-Feng Li − *Department of Materials Engineering, Ming Chi University of Technology, New Taipei City 24301, Taiwan; Department of Materials Science and Engineering, National Taiwan University, Taipei 10617, Taiwan*

Shih-Han Cheng − *Department of Materials Engineering, Ming Chi University of Technology, New Taipei City 24301, Taiwan*

Hou-Chin Cha − *College of Engineering & Organic Electronics Research Center, Ming Chi University of Technology, New Taipei City 24301, Taiwan*

Ssu-Yung Chung − *Department of Materials Engineering, Ming Chi University of Technology, New Taipei City 24301, Taiwan*

Damian Glowienka − *Faculty of Applied Physics and Mathematics, Gdańsk University of Technology, Gdańsk 80-233, Poland;* orcid.org/0000-0001-5508-2929

Chih-Min Chuang − *Department of Physics, National Atomic Research Institute, Taoyuan 325207, Taiwan*

Complete contact information is available at: https://pubs.acs.org/10.1021/acsaem.4c02521

Author Contributions

Y.-C.H. designed, analyzed, drafted, and proofread this research; C.-F.L., S.-H.C., and S.-Y.C. conducted the experiments; C.-F.L., H.-C.C., D.G., and C.-M.C. analyzed the data and composed the manuscript.

Notes

The authors declare no competing financial interest.

■ ACKNOWLEDGMENTS

This research was supported in full by the National Science and Technology Council of Taiwan (Grants NSTC 112-2628-E-131-001-MY4 and NSTC 107-2218-E-131-007-MY3). This research was partly funded by the National Science Centre, in cooperation with the M-ERA.NET 3 Call 2021 for Grant 2021/03/Y/ST5/00233. This project has received funding from the European Union's Horizon 2020 research and innovation program under Grant Agreement 958174.

■ REFERENCES

(1) Cui, Y.; Xu, Y.; Yao, H.; Bi, P.; Hong, L.; Zhang, J.; Zu, Y.; Zhang, T.; Qin, J.; Ren, J.; et al. Single-junction organic photovoltaic cell with 19% efficiency. *Adv. Mater.* **2021**, *33* (41), No. 2102420.

(2) Huang, Y.-C.; Cha, H.-C.; Huang, S.-H.; Li, C.-F.; Santiago, S. R. M.; Tsao, C.-S. Highly Efficient Flexible Roll-to-Roll Organic Photovoltaics Based on Non-Fullerene Acceptors. *Polymers* **2023**, *15* (19), 4005.

(3) Li, Y.; Huang, X.; Ding, K.; Sheriff, H. K., Jr.; Ye, L.; Liu, H.; Li, C.-Z.; Ade, H.; Forrest, S. R. Non-fullerene acceptor organic photovoltaics with intrinsic operational lifetimes over 30 years. *Nat. Commun.* **2021**, *12* (1), 5419.

(4) Zhou, D.; Wang, J.; Xu, Z.; Xu, H.; Quan, J.; Deng, J.; Li, Y.; Tong, Y.; Hu, B.; Chen, L. Recent advances of nonfullerene acceptors in organic solar cells. *Nano Energy* **2022**, *103*, No. 107802.

(5) Sun, H.; Chen, F.; Chen, Z.-K. Recent progress on non-fullerene acceptors for organic photovoltaics. *Mater. Today* **2019**, *24*, 94−118.

(6) Datt, R.; Lee, H. K. H.; Spence, M.; Carnie, M.; Tsoi, W. C. High performance non-fullerene organic photovoltaics under implant light illumination region. *Appl. Phys. Lett.* **2023**, *122* (14), No. 143906.

(7) Solak, E. K.; Irmak, E. Advances in organic photovoltaic cells: a comprehensive review of materials, technologies, and performance. *RSC Adv.* **2023**, *13* (18), 12244−12269.

(8) Tan, L. C.; Wang, Y. L.; Zhang, J. W.; Xiao, S. Q.; Zhou, H. Y.; Li, Y. W.; Chen, Y. W.; Li, Y. F. Highly Efficient Flexible Polymer Solar Cells with Robust Mechanical Stability. *Adv. Sci.* **2019**, *6* (7), 8.

(9) Karki, A.; Vollbrecht, J.; Gillett, A. J.; Xiao, S. S.; Yang, Y.; Peng, Z.; Schopp, N.; Dixon, A. L.; Yoon, S.; Schrock, M.; et al. The role of bulk and interfacial morphology in charge generation, recombination, and extraction in non-fullerene acceptor organic solar cells. *Energ Environ. Sci.* **2020**, *13* (10), 3679−3692.

(10) Graham, K. R.; Cabanetos, C.; Jahnke, J. P.; Idso, M. N.; El Labban, A.; Ngongang Ndjawa, G. O.; Heumueller, T.; Vandewal, K.; Salleo, A.; Chmelka, B. F.; et al. Importance of the Donor:Fullerene Intermolecular Arrangement for High-Efficiency Organic Photovoltaics. *J. Am. Chem. Soc.* **2014**, *136* (27), 9608−9618.

(11) Cao, B.; He, X.; Fetterly, C. R.; Olsen, B. C.; Luber, E. J.; Buriak, J. M. Role of Interfacial Layers in Organic Solar Cells: Energy Level Pinning versus Phase Segregation. *ACS Appl. Mater. Interfaces* **2016**, *8* (28), 18238−18248.

(12) Yin, Z.; Wei, J.; Zheng, Q. Interfacial Materials for Organic Solar Cells: Recent Advances and Perspectives. *Adv. Sci.* **2016**, *3* (8), No. 1500362.

(13) Simokaitiene, J.; Cekaviciute, M.; Volyniuk, D.; Sini, G.; Voz, C.; Puigdollers, J.; Bucinskas, A.; Grazulevicius, J. V. Satisfying both interfacial- and bulk requirements for organic photovoltaics: Bridged-triphenylamines with extended π-conjugated systems as efficient new molecules. *Org. Electron.* **2019**, *73*, 137−145.

(14) Luke, J.; Yang, E. J.; Chin, Y.-C.; Che, Y.; Winkler, L.; Whatling, D.; Labanti, C.; Park, S. Y.; Kim, J.-S. Strong Intermolecular Interactions Induced by High Quadrupole Moments Enable Excellent Photostability of Non-Fullerene Acceptors for Organic Photovoltaics. *Adv. Energy Mater.* **2022**, *12* (30), No. 2201267.

(15) Li, P.; Cai, L.; Wang, G.; Zhou, D. C.; Xiang, J.; Zhang, Y. J.; Ding, B. F.; Alameh, K.; Song, Q. L. PEIE capped ZnO as cathode buffer layer with enhanced charge transfer ability for high efficiency polymer solar cells. *Synth. Met.* **2015**, *203*, 243−248.

(16) Ling, Z.; Zhao, Y.; Wang, S.; Pan, S.; Lian, H.; Peng, C.; Yang, X.; Liao, Y.; Lan, W.; Wei, B.; Chen, G. High-performance light-soaking-free polymer solar cells based on a LiF modified ZnO electron extraction layer. *J. Mater. Chem. C* **2019**, *7* (30), 9354−9361.

(17) Sung, Y.-M.; Chang, C.-H.-T.; Tsao, C.-S.; Lin, H.-K.; Cha, H.-C.; Jiang, P.-C.; Liu, T.-C.; Chang, K.-W.; Huang, Y.-C.; Tsay, J.-S. Dramatic improvement in the stability and mechanism of high-performance inverted polymer solar cells featuring a solution-processed buffer layer. *Nanoscale* **2023**, *15* (7), 3375−3386.

(18) Zhang, B.; Bonner, J. C.; Murthy, L. N.; Nguyen, T. A.; Cao, F.-Y.; Cheng, Y.-J.; Hamadani, B. H.; Hsu, J. W. Color-temperature dependence of indoor organic photovoltaic performance. *Org. Electron.* **2022**, *104*, No. 106477.

(19) Wu, J.; Gao, M.; Chai, Y.; Liu, P.; Zhang, B.; Liu, J.; Ye, L. Towards a bright future: The versatile applications of organic solar cells. *Mater. Rep.: Energy* **2021**, *1* (4), No. 100062.

(20) Bai, F.; Zhang, J.; Zeng, A.; Zhao, H.; Duan, K.; Yu, H.; Cheng, K.; Chai, G.; Chen, Y.; Liang, J.; et al. A highly crystalline non-fullerene acceptor enabling efficient indoor organic photovoltaics with high EQE and fill factor. *Joule* **2021**, *5* (5), 1231−1245.

(21) Alkhalayfeh, M. A.; Abdul Aziz, A.; Pakhuruddin, M. Z.; Katubi, K. M. M.; Ahmadi, N. Recent Development of Indoor Organic Photovoltaics. *Phys. Status Solidi A* **2022**, *219* (5), No. 2100639.

(22) Yang, Z.; Guan, C.; Jiang, X.; Zhang, G.; Xie, C.; Liu, C.; Xiao, C.; Li, W. High-Performance Indoor Organic Solar Cells Based on a Double-Cable Conjugated Polymer. *Sol. RRL* **2022**, *6* (6), No. 2100981.

(23) Li, X.; Xiao, C.; Yang, Z.; Wang, H.; Liu, B.; Tan, W. L.; Chen, Q.; Wang, C.; McNeill, C. R.; Li, W. Indoor Single-Component Organic Solar Cells Based on Double-Cable Conjugated Polymers with Pendant A-π-D-π-A Electron Acceptors. *Sol. RRL* **2023**, *7* (13), No. 2300241.

(24) Lee, C.; Lee, J. H.; Lee, H. H.; Nam, M.; Ko, D. H. Over 30% Efficient Indoor Organic Photovoltaics Enabled by Morphological

Modification Using Two Compatible Non-Fullerene Acceptors. *Adv. Energy Mater.* **2022**, *12* (22), No. 2200275.
(25) Ma, L.-K.; Chen, Y.; Chow, P. C. Y.; Zhang, G.; Huang, J.; Ma, C.; Zhang, J.; Yin, H.; Hong Cheung, A. M.; Wong, K. S.; et al. High-Efficiency Indoor Organic Photovoltaics with a Band-Aligned Interlayer. *Joule* **2020**, *4* (7), 1486−1500.
(26) Kumar, G.; Chen, F.-C. A review on recent progress in organic photovoltaic devices for indoor applications. *J. Phys. D. Appl. Phys.* **2023**, *56* (35), No. 353001.
(27) Xu, X.; Liu, W.; Luo, X.; Chen, H.; Wei, Q.; Yuan, J.; Zou, Y. An Overview of High-Performance Indoor Organic Photovoltaics. *ChemSusChem* **2021**, *14* (17), 3428−3448.
(28) Wang, K.-L.; Zhou, Y.-H.; Lou, Y.-H.; Wang, Z.-K. Perovskite indoor photovoltaics: opportunity and challenges. *Chem. Sci.* **2021**, *12* (36), 11936−11954.
(29) Chen, Z.; Wang, T.; Wen, Z.; Lu, P.; Qin, W.; Yin, H.; Hao, X.-T. Trap State Induced Recombination Effects on Indoor Organic Photovoltaic Cells. *ACS Energy Lett.* **2021**, *6* (9), 3203−3211.
(30) Ylikunnari, M.; Valimaki, M.; Vaisanen, K.-L.; Kraft, T. M; Sliz, R.; Corso, G.; Po, R.; Barbieri, R.; Carbonera, C.; Gorni, G.; Vilkman, M. Flexible OPV modules for highly efficient indoor applications. *Flex. Print. Electron.* **2020**, *5* (1), No. 014008.
(31) Huang, Y.-C.; Li, C.-F. Insights into the photovoltaic mechanism of organic photovoltaics under solar and artificial light. *J. Mater. Chem. C* **2023**, *11* (41), 14079−14087.
(32) Yang, S. S.; Hsieh, Z. C.; Keshtov, M. L.; Sharma, G. D.; Chen, F. C. Toward High-Performance Polymer Photovoltaic Devices for Low-Power Indoor Applications. *Sol. RRL* **2017**, *1* (12), 6.
(33) Cui, Y.; Wang, Y.; Bergqvist, J.; Yao, H.; Xu, Y.; Gao, B.; Yang, C.; Zhang, S.; Inganäs, O.; Gao, F.; et al. Wide-gap non-fullerene acceptor enabling high-performance organic photovoltaic cells for indoor applications. *Nat. Energy* **2019**, *4* (9), 768−775.
(34) Xie, C.; Xiao, C.; Fang, J.; Zhao, C.; Li, W. Core/shell AgNWs@ SnOx electrodes for high performance flexible indoor organic solar cells with> 25% efficiency. *Nano Energy* **2023**, *107*, No. 108153.
(35) Sung, Y.-M.; Akbar, A. K.; Biring, S.; Li, C.-F.; Huang, Y.-C.; Liu, S.-W. The effect of ZnO preparation on the performance of inverted polymer solar cells under one sun and indoor light. *J. Mater. Chem. C* **2021**, *9*, 1196−1204.
(36) Chaturvedi, N.; Gasparini, N.; Corzo, D.; Bertrandie, J.; Wehbe, N.; Troughton, J.; Baran, D. All slot-die coated non-fullerene organic solar cells with PCE 11%. *Adv. Funct. Mater.* **2021**, *31* (14), No. 2009996.
(37) Sung, Y.-M.; Tsao, C.-S.; Lin, H.-K.; Cha, H.-C.; Huang, Y.-C. Scale-up fabrication and characteristic study of oligomer-like small-molecule solar cells by ambient halogen-free sheet-to-sheet and roll-to-roll slot-die coating. *Sol. Energy* **2022**, *231*, 536−545.
(38) Myung, J. H.; Kim, S.-J.; Kim, H.; Yun, C.; Kang, M. H. Scalable fabrication of flexible large-area inverted organic photovoltaic cells. *J. Semicond. Technol. Sci.* **2021**, *21* (3), 215−221.
(39) Tsai, C.-Y.; Lin, Y.-H.; Chang, Y.-M.; Kao, J.-C.; Liang, Y.-C.; Liu, C.-C.; Qiu, J.; Wu, L.; Liao, C.-Y.; Tan, H.-S.; et al. Large area organic photovoltaic modules fabricated on a 30 cm by 20 cm substrate with a power conversion efficiency of 9.5%. *Sol. Energy Mater. Sol. Cells* **2020**, *218*, No. 110762.
(40) Basu, R.; Gumpert, F.; Lohbreier, J.; Morin, P.-O.; Vohra, V.; Liu, Y.; Zhou, Y.; Brabec, C. J.; Egelhaaf, H.-J.; Distler, A. Large-area organic photovoltaic modules with 14.5% certified world record efficiency. *Joule* **2024**, *8* (4), 970−978.
(41) Gumpert, F.; Janßen, A.; Basu, R.; Brabec, C. J.; Egelhaaf, H.-J.; Lohbreier, J.; Distler, A. On the theoretical framework for meniscus-guided manufacturing of large-area OPV modules. *Prog. Org. Coat.* **2024**, *192*, No. 108505.
(42) Kim, D. H.; Wibowo, F. T.; Lee, D.; Krishna, N. V.; Park, S.; Cho, S.; Jang, S. Y. Non-Fullerene-Based Inverted Organic Photovoltaic Device with Long-Term Stability. *Energy Environ. Mater.* **2023**, *6* (3), No. e12381.
(43) Park, S.; Kim, T.; Yoon, S.; Koh, C. W.; Woo, H. Y.; Son, H. J. Progress in Materials, Solution Processes, and Long-Term Stability for Large-Area Organic Photovoltaics. *Adv. Mater.* **2020**, *32* (51), No. 2002217.
(44) Kim, T. H.; Park, N. W.; Saeed, M. A.; Jeong, S. Y.; Woo, H. Y.; Park, J.; Shim, J. W. Record indoor performance of organic photovoltaics with long-term stability enabled by self-assembled monolayer-based interface management. *Nano Energy* **2023**, *112*, No. 108429.
(45) Mitra, K. Y.; Alalawe, A.; Voigt, S.; Boeffel, C.; Baumann, R. R. Manufacturing of all inkjet-printed organic photovoltaic cell arrays and evaluating their suitability for flexible electronics. *Micromachines* **2018**, *9* (12), 642.
(46) Che, X.; Li, Y.; Qu, Y.; Forrest, S. R. High fabrication yield organic tandem photovoltaics combining vacuum-and solution-processed subcells with 15% efficiency. *Nat. Energy* **2018**, *3* (5), 422−427.
(47) Cha, H.-C.; Huang, Y.-C.; Li, C.-F.; Tsao, C.-S. Uniformity and process stability of the slot-die coated PTB7: PC71BM organic photovoltaic improved by solvent additives. *Mater. Chem. Phys.* **2023**, *302*, No. 127684.
(48) Sygusch, J.; Rudolph, M. A contribution to wettability and wetting characterisation of ultrafine particles with varying shape and degree of hydrophobization. *Appl. Surf. Sci.* **2021**, *566*, No. 150725.
(49) Kalgudi, S.; Pavithra, G. P.; Prabhu, K. N.; Koppad, P. G.; Venkate Gowda, C.; Satyanarayan. Effect of surface treatment on wetting behavior of copper. *Mater. Today Proc.* **2021**, *35*, 295−297.
(50) Jakubka, F.; Heyder, M.; Machui, F.; Kaschta, J.; Eggerath, D.; Lövenich, W.; Krebs, F. C.; Brabec, C. J. Determining the coating speed limitations for organic photovoltaic inks. *Sol. Energy Mater. Sol. Cells* **2013**, *109*, 120−125.
(51) Pockett, A.; Lee, H. K. H.; Coles, B. L.; Tsoi, W. C.; Carnie, M. J. A combined transient photovoltage and impedance spectroscopy approach for a comprehensive study of interlayer degradation in non-fullerene acceptor organic solar cells. *Nanoscale* **2019**, *11* (22), 10872−10883.
(52) Hailegnaw, B.; Sariciftci, N. S.; Scharber, M. C. Impedance Spectroscopy of Perovskite Solar Cells: Studying the Dynamics of Charge Carriers Before and After Continuous Operation. *Phys. Status Solidi A-Appl. Mater.* **2020**, *217* (22), No. 2000291.
(53) Hora, J.; Hall, C.; Evans, D.; Charrault, E. Inorganic Thin Film Deposition and Application on Organic Polymer Substrates. *Adv. Eng. Mater.* **2018**, *20* (5), No. 1700868.
(54) Zhang, Y.; Li, X.; Dai, T.; Xu, D.; Xi, J.; Chen, X. Charge transport and extraction of PTB7:PC71BM organic solar cells: effect of film thickness and thermal-annealing. *RSC Adv.* **2019**, *9* (43), 24895−24903.
(55) Liu, Z.; Wang, N. Small Energy Loss and Broad Energy Levels Offsets Lead to Efficient Ternary Polymer Solar Cells from a Blend of Two Fullerene-Free Small Molecules as Electron Acceptors. *Adv. Opt. Mater.* **2019**, *7* (21), No. 1900913.

https://doi.org/10.1021/acsaem.4c02521
ACS Appl. Energy Mater. 2024, 7, 10203−10211